Materials Today Bio 24 (2024) 100895

Contents lists available at ScienceDirect

Materials Today Bio

journal homepage: www.journals.elsevier.com/materials-today-bio

Enhanced EPR effects by tumour stromal cell mimicking nanoplatform on invasive pituitary adenoma

Junning Ma [a,b,c,d,e,1,*], Yin Wei [a,1], Xiaojian Zhang [b,d,1], Lu Lin [b,d,1], Youmei Bao [f,1], Hui Cao [c,1], Honghwei Chen [c,1], Jianbo Yu [c,1], Jiqi Yang [c,1], Yue Zhang [b,d,1], Huimin Lan [b,d,1], XueYang Li [b,d,1], Huang Qiong [a,1], Dan Yang [a,1], Yajun Yu [a,1], Jingyao Chen [a,1], Chengchen Zhang [a,1], Li liu [a,1], Lei Chen [b,d,1], Renya Zhan [a,c,1,**], Fei Liu [b,d,1,***]

[a] Zhejiang University School of Medicine, Zhe Jiang, 310003, China
[b] Department of Neurosurgery of Fifth affiliated Hospital, SunYat-Sen University Zhuhai, 519000, ZhuHai, China
[c] Department of Neurosurgery of First affiliated Hospital, Zhejiang University School of Medicine Hangzhou, Zhe Jiang, 310003, China
[d] Sun Yat-Sen University, Guangzhou, 510275, China
[e] Department of Pathology& Pathophysiology and Department of Surgical Oncology of Second Affiliated Hospital, Zhejiang University School of Medicine, Zhe Jiang, 310003, China
[f] School of Medicine Yale University, New Haven, CT, 06510, USA

ARTICLE INFO

Keywords:
Gap junction
Tumour microenvironment
Folliculostellate cell
Nanoparticle
Invasive pituitary adenoma

ABSTRACT

Rapid advances in nanomedicine have enabled potential applications in cancer therapy. The enhanced permeability and retention (EPR) effect is the primary rationale for the passive targeting of nanoparticles in oncology. However, growing evidence indicates that the accumulation of nanomaterials via the EPR effect could be more efficient. Inspired by our clinical observation of the Gap Junction connecpion between folliculostellate cells and pituitary adenoma cells, we designed a novel drug delivery system that targets tumours by coating folliculostellate cell (FS) membranes onto PLGA nanoparticles (NPs). The resulting FSNPs, inheriting membrane proteins from the folliculostellate cell membrane, significantly enhanced the EPR effect compared to nanoparticles without cancer cell membranes. We further demonstrated that mitotane encapsulation improved the therapeutic efficacy of mitotane in both heterotopic and orthotopic pituitary adenoma models. Owing to its significant efficacy, our FS cell membrane-coated nanoplatforms has the potential to be translated into clinical applications for the treatment of invasive pituitary adenoma.

1. Introduction

The role of the tumour microenvironment is critical in the development of active anticancer therapeutics [1]. The tumour microenvironment comprises tumour cells surrounded by various tumour stromal cells and extracellular matrix. Stromal cells maintain cancer stem cells and form metastatic niches to regulate cancer cell progression [2]. Conversely, morphological evidence from reactive tumour stroma has shown that tumour cells can change their adjacent stroma to form a permissive and supportive environment for cancer growth [3]. In addition, by sharing various soluble and membrane-bound mediators based on the tissue context and tumour type, the interaction between stroma and cancer cells can affect the sensitivity of tumours to various therapeutics. Unfortunately, most attempts at manipulating the tumour microenvironment failed during Phase III trials due to low efficacy [4,5]. Limited success in the clinical translation of preclinical efficacy studies poses an urgent need for new strategies to improve the efficacy of current cancer therapy [6–9].

The rapid development of nanotechnology for drug delivery has led to the development of nanoparticles tailored to improve the therapeutic outcomes of various cancers [10–12]. Fundamentally, an active targeting strategy by conjugating antibodies or ligands on the surface of

* Corresponding author. Zhejiang University School of Medicine, Zhe Jiang, 310003, China.
** Corresponding author. Zhejiang University School of Medicine, Zhe Jiang, 310003, China.
*** Corresponding author. Department of Neurosurgery of Fifth affiliated Hospital, SunYat-Sen University Zhuhai, 519000, ZhuHai, China.
E-mail addresses: 0620542@zju.edu.cn (J. Ma), 1196057@zju.edu.cn (R. Zhan), doctorlf@126.com (F. Liu).
[1] These authours contributed equally to this work.

https://doi.org/10.1016/j.mtbio.2023.100895
Received 20 August 2022; Received in revised form 22 November 2023; Accepted 29 November 2023
Available online 18 December 2023

nanoparticles and a passive targeting strategy by the leaky nature of tumour vessels results in enhanced permeability and retention (EPR) effects; nanoparticles can be navigated specifically into solid tumour tissue [9,11,13,14]. However, before targeting ligands bind to cancer cells, actively targeted nanomedicines must be cleared from the bloodstream and hindered by the binding site barrier [11,15,16]. Growing evidence has pointed out that accumulation of nanomaterials in tumour tissues does not reach 5 % [13,17,18]. Because of the high heterogeneity of the pathophysiological conditions in the tumour microenvironment, EPR effects have received increasing criticism in recent years [11,17].

Cell membrane-coated nanotechnology is a powerful bionic strategy for nanoparticle engineering [19,20]. By simply coating the cell membrane, multiple bio-interfacing capabilities of the donor cell membrane can be imparted to the nanoparticles [19,21–24]. Folliculostellate (FS) cells are resident, sustentacular-like, non-endocrine, complementary populations in the anterior pituitary [25].

FS cells are the main functional cells in the normal anterior pituitary gland, regulating hormone secretion [26]. Under pathological conditions, FS neurones function as stoma cells in the microenvironment of the pituitary adenoma and are involved in basement membrane remodelling, tumoural neoangiogenesis, and tumoural expansion [25,27]. Meanwhile, clinical evidence from patients with pituitary adenoma has shown that FS neurons form network-like structures and are frequently in close relationship with cancer cells through adjacent and gap junctions [28,29].

Gap junctions comprise arrays of intercellular channels formed by connexin proteins that provide direct communication between adjacent cells. This type of intercellular communication permits the coordination of cellular activities and plays key role in controlling cell growth and differentiation and maintaining tissue homeostasis [30]. Inspired by the nature of the bidirectional interaction between FS neurones and tumour cells from pathological discoveries in patients with pituitary adenoma, we developed a pituitary tumour cell-oriented delivery platform by coating the FS neuron membrane onto PLGA nanoparticles (Fig. 1). FS and tumour stem cells were isolated from surgically removed tumour tissues of patients with invasive pituitary adenoma. FS neurones were cultured to fabricate nanoparticles, and tumour stem cells were prepared for heterotopic and orthotopic animal models. It was demonstrated that FS cell membrane modification could enhance the EPR effect of nanoparticles, leading to specific targeting efficiency in tumours, both heterotopically and orthotopically. Furthermore, when loaded with mitotane to induce tumour cell apoptosis, FSNPs achieved significantly suppressed tumour growth in a therapeutic setting.

2. Materials and methods

2.1. Tumour tissue resection by transsphenoidal surgery from patients with invasive pituitary adenoma

Transsphenoidal procedures were performed by neurosurgeons under MR neuronavigation guidance. Patient's upper body was elevated by 15 °C, and the head was fixed in a Sugita 4-point head holder (Mizuho Medical Innovation, Tokyo, Japan) and rotated to the operator's side by 10–20° after anaesthesia. A vertical incision was made in the nasal septal mucosa of the right nostril and dissected between the periosteum and septal bones. The septal bone was carefully removed to expose its anterior wall. The sphenoidal bone and the septal wall were opened widely without damaging the contralateral mucosa. Next, the sellar floor was opened to expose the dura rostrally to the tuberculum sellae and the cavernous sinuses bilaterally. The tumours were exposed and removed for pathological diagnosis. Some tumours were immediately fixed with glutaraldehyde for transmission electron microscopy. Half of the tumour tissue was kept on ice for tumour stem cell and FS neuron isolation. After the tumour was removed, the floor was reconstructed by suturing the dura with abdominal fat or fascia and spraying it stellar with fibrin.

2.2. Isolation and culture of human tumour stem cells, FS cells, and tumour-associated fibroblasts

Human tumour stem cells were isolated according to previously reported procedures [31,32].

Briefly, tumour tissues were dissected into 1 mm^3 pieces and washed in PBS 3 times after surgical resection within 30 min. After digestion in papain for 15 min at 37 °C, tumour samples were triturated by passing them in a tissue sieve and passed through a 70 μm cell strainer. Cell suspensions were transferred to six-well plates and cultured in DMEM/F12 medium (Gibco, Carlsbad, CA, USA) supplemented with 10 % B27 (Gibco), penicillin/streptomycin (200 U/ml, Gibco), EGF (40 ng/ml, Peprotech, Cranbury, NJ, USA), and bFGF (40 ng/ml, Peprotech). For fluorescence active cell sorting, a single-cell suspension of tumour tissue

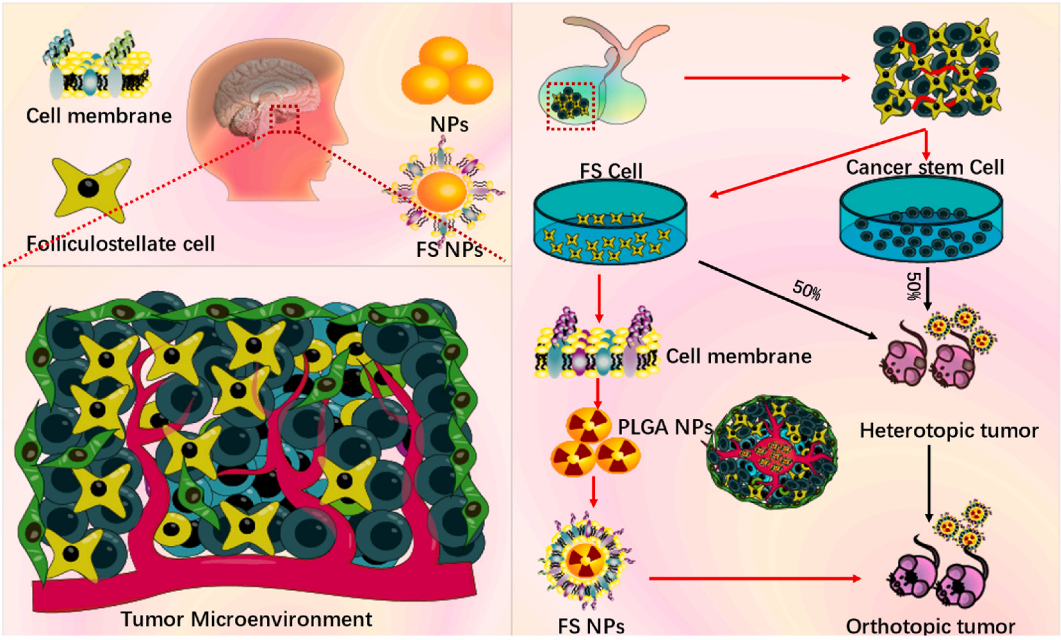

Fig. 1. Schematic illustration of pituitary adenoma tumour stem cell navigated FSNPs for Invasive pituitary adenoma.

was washed with PBS and resuspended in FACS buffer with anti-CD133 antibody conjugated to APC and anti-S100 antibody conjugated to PE on ice for 30 min (BioLegend, San Diego, CA, USA). After incubation, the cells were washed with FACS buffer three times to remove unconjugated antibodies. The final cell pellet was resuspended in 200ul of FACS buffer for cell sorting. After sorting, cells were washed with DMEM medium and cultured in DMEM supplemented with 10 % FBS and 200U/ml penicillin/streptomycin at 37 °C in a humidified atmosphere with 5 % CO_2. For isolating and culture of tumour-associated fibroblasts, single-cell cells suspension of tumour tissue was seeded in 6 wells plate with DMEM medium supplemented with 10 % FBS, 1 % NEAA (Hyclone, Logan, UT, USA), 1 % sodium pyruvate (Hyclone) at 37 °C with 5 % CO_2.

2.3. Preparation of cell membrane

The cell membrane preparation process was performed by hypotonic lysis and repeated freeze-thaw processes with minor modifications according to our previously reported procedures [21,33]. Briefly, FS neurones were resuspended in 1 ml lysing buffer containing EDTA-free protease inhibitor, 10 mM Tris, and 10 mM MgCl2 for 3 h on ice. Next, cell homogenate was suffered by a freeze-thaw process at least 5 times, followed by centrifugation at 7000×*g* for 10 min at 4 °C. The supernatant was centrifuged at 13,000×*g* for 60 min. The resulting precipitate was resuspended in 1 ml Dnase-free/Rnase-free water (Invitrogen, Carlsbad, CA, USA) and stored at −80 °C until use.

2.4. Synthesis of PLGA NPs and FS cell membrane-coated NPs

PLGA NPs were synthesised according to previously reported procedures [33–35]. Briefly, 50 mg of PLGA polymer and cargo agent were dissolved in 1 ml ethyl acetate. The solution was then added dropwise to a tube containing 2 ml 2.5 % polyvinyl alcohol (PVA, MW 30,000–70,000) under vortexing and ultrasonication to form an oil/water solution. The solution was poured into a beaker with 35 ml 0.3 % PVA and stirred at 520 rpm overnight at 4 °C. The NPs were collected by centrifugation at 18,000 rpm for 20 min and washed with water. To form FS cell membrane coated PLGA NPs, 0.5 ml PLGA NPs and 0.5 ml cell membrane suspension were mixed in a 1 ml syringe (Hamilton, Reno, NV, USA) and extruded through a 200 nm membrane filter (Whatman, Maidstone, United Kingdom) in a mechanical extruder 7 times.

2.5. Scanning electron microscopy (SEM)

The morphology of nanoformulations was observed by SEM. Briefly, a carbon tape containing lyophilized NPs was coated with gold using a sputter set at 40 mA (Dynavac Mini Coater, Dynavac, Hingham, MA, USA). All images were obtained using a LaB electron gun with a Philips XL 30 SEM at an accelerating voltage of 5 kV.

2.6. Transmission electron microscope (TEM)

TEM was used to observe the structure of nanoparticles. One drop of the nanoparticle suspension was placed on a glow-discharged carbon-coated grid. Nanoparticles were then rinsed with five drops of distilled water for 3 min. Phosphotungstic acid was added to the sample, followed by washing with ddH_2O. Images were captured using a spherical microscope (FEI 200 kV parameter.

2.7. Dynamic light scattering (DLS)

The hydrodynamic size and zeta potential surface charge were measured using a scattering system. Briefly, 0.1 mg of NPs, FNPs, and FSNPs were dissolved in 1 ml ddH_2O, poured into a transparent cuvette, and measured using a Malvern Zetasizer.

2.8. Characterization of loading and release of mitotane

High-performance liquid chromatography (HPLC) was used to measure the mitotane loading efficiency of the NPs. Briefly, 1 mg of mitotane-encapsulated FSNPs was incubated in 1 ml methanol and sonicated for 5 min, followed by centrifugation at 17,500 rpm for 15 min. The supernatants were collected for HPLC analysis. The loading efficiency was calculated using the following formula: loading efficiency = (total mitotane-free mitotane)/total Mitotane x100 %.

To determine the release, 1 mg of lyophilized mitotane-loaded FSNPs was dissolved in 1 ml ddH_2O in Eppendorf tubes. The tubes were kept at 37 °C in an incubator and shaken at a speed of 150 cycles per minute. At selected time points, the tubes were centrifuged at 17,500 rpm for 10 min. The supernatants were collected for mitotane analysis. The pellet was resuspended in 1 ml ddH_2O. For the HPLC analysis, a mobile phase consisting of 40 % buffer (50 mM $NH_4H_2PO_4$) and 60 % acetonitrile was pumped at a flow rate of 1 ml per minute. Detection was performed using a UV detector (Shimadzu RF-10A, Kyoto, Japan) at an absorbance wavelength of 226 nm.

2.9. Lentivirus transduction of luciferase

Lentivirus production and transduction were performed according to our previous report [36]. Briefly, lentiviruses were harvested from the supernatant of 293 T cells culture medium without FBS at 3–4 days after the introduction of plasmids PCDH-CMV-Nluc, PsPAX2, and pMD2.G. Tumour stem cells with stable gene overexpression were obtained through antibiotic selection using puromycin at 3ug/ml.

2.10. In vitro mimic of tumour microenvironmental vasculature system

The transwell co-culture system was established as previously reported with minor modifications. Briefly, stem cells were cultured in DMEM/F12 containing 10 % B27, penicillin/streptomycin (200U/ml-, Gibco), EGF (40 ng/ml), and bFGF (40 ng/ml) at 24 wells plate. Next, transwell inserts were coated with Matrigel, and Huvec cells were seeded at the bottom of inserts in the M200 medium (Life Technologies, Carlsbad, CA, USA) containing 10 % FBS,1 % Pen/Strep (Life Technologies), and growth factors (LSGS, Life Technologies) at 37 °C in a humidified atmosphere with 5 % CO_2 for 24 h. One hundred ug of rhodamine-loaded nanoformulations were added in the up chamber of the transwell system. After 4 h of incubation, cells from the bottom chamber were analysed by flow cytometry. A 6 mm coverslip coated with 0.01 % poly-L-lysine was placed in the bottom 24 wells plate for immunocytochemistry staining.

2.11. Tumour inoculation

All animal experiments were approved by the Zhejiang University Institutional Animal Care and Utilization Committee. All efforts were made to minimise suffering during each experiment. Tumour stem cells were digested into single cells and implanted into four-to six-week female nude mice (Charles River Laboratories, Wilmington, MA, USA). To establish a heterotopic invasive pituitary adenoma model, the mice were injected with $1x10^6$ tumour stem cells in the flank. Tumour size was measured every 2–3 days (length × width) using a caliper. The tumour volume was determined using the formula length × width × width/2. For orthotopic Invasive pituitary adenoma, mice were anaesthetised and injected with 6.0×10^5 tumour stem cells in the right striatum, which were engineered to express luciferase in a total volume of 3uL of physiologic saline at a rate of 0.2 μL/minute. Injection coordinates were 2.5 mm lateral and 0.5 mm anterior to the bregma at a depth of 3 mm from the cortical surface. The development of pituitary adenomas in the brain was monitored using an IVIS system (Xenogen, Caliper Life Sciences, Hopkinton, MA, USA).

2.12. Fluorescent imaging

Tumour-bearing mice were randomly assigned to experimental groups (n = 3). Each group received IR780-loaded nanoparticles intravenously via tail vein injections. Before nanoparticle administration, the nanoparticle dose was adjusted to ensure that the same amount of IR-780 was injected into each group by fluorescence intensity normalisation. Mice were sacrificed 24 h later. Tumour tissue and main organs were collected and imaged by IVIS with excitation wavelength of 745 nm and emission wavelength of 820 nm for IR780-loaded NPs. The fluorescence intensity of each tissue was quantified using Living Image 3.0 software (Caliper Life Sciences, Hopkinton, MA, USA).

2.13. Fluorescent immunohistochemistry for ACTH

Twenty-four hours after administering coumarin-6 loaded nanoformulations, mice were perfused with PBS after anaesthesia, followed by fixation with 4 % paraformaldehyde. The tumours were dissected, placed in 4 % paraformaldehyde for 2 days, and transferred into 30 % sucrose. Tumour were sliced at 30um by cryostat section after fixation. The sections were treated with 0.1 % Triton X-100, transferred to 24 cell culture plates, and wash process for 3 times. After blocking with 4 % BSA for 30 min, the cells were washed 3 times. Then, sections were incubated with anti-ACTH antibody (1:500) (BioLegend, San Diego, CA, USA) overnight at 4 °C, followed by incubation with rabbit anti-mouse IgG (Santa Cruz Biotechnology, Dallas, TX, USA) for 30 min. The samples were mounted with DAPI and imaged using a confocal microscope (Leica TCS SP8).

2.14. Statistical analysis

Data from *in vitro* experiments are presented as mean and standard deviation. Comparisons between the groups were performed using t-tests. One-way analysis was used to compare the statistical significance of various treatment. Statistical analyses were conducted with GraphPad Prism7.0. *P < 0.05, **P < 0.01, ***P < 0.001, and ****P < 0.0001 were considered significant.

3. Result and discussion

3.1. Clinical case of invasive pituitary adenoma

A pituitary adenoma is caused by a tumour originating from the corticotrophic cells of the pituitary gland, which leads to excess hormones [37,38]. Herein, a case of invasive pituitary adenoma was diagnosed using MRI (Hardy classification, grade IV; Knosp classification, grade 4) (Fig. 2A–D). Pathological examination of the resected tumour tissue revealed representative acinar cells with high ACTH (Fig. 2 E and F). Furthermore, we examined the expression of S-100 and strong staining for CD133 in tumour tissues to detect the density of FS neurones and tumour stem cells using immunohistochemistry (Fig. 2 G and H).

3.2. Preparation and characterization of FSNPs

Our patient underwent transsphenoidal surgery to remove the tumour (Fig. 3A). A part of the tumour section was sent for microstructural examination using TEM. Gap junctions (red arrow in the insert) were found between FS neurones and tumour cells (Fig. 3 B, Figure S1A), indicating the important role of FS neurones in tumourigenesis-related processes [25]. Emerging evidence indicates that connexins play key roles in cancer stem cell biology [30]. Intrigued by the evidence from Immunohistochemistry and TEM, we simultaneously isolated FS neurones and tumour stem cells from tumour tissue. After purification by fluorescence-activated cell sorting, FS neurones and tumour stem cells were sorted using the markers S100+ and CD133- (Fig. 3C and Supplemental Figure 1 B) and expanded in DMEM with foetal calf serum for cell membrane preparation. Tumour stem cells expressing S100 and CD133 (Figure D and Supplemental Figure C) were expanded in a serum-free medium containing growth factors and B27 to build ex situ and in situ pituitary tumour models.

Bidirectional interactions through gap junctions between FS neurones and tumour stem cells mainly rely on connexin molecules from the

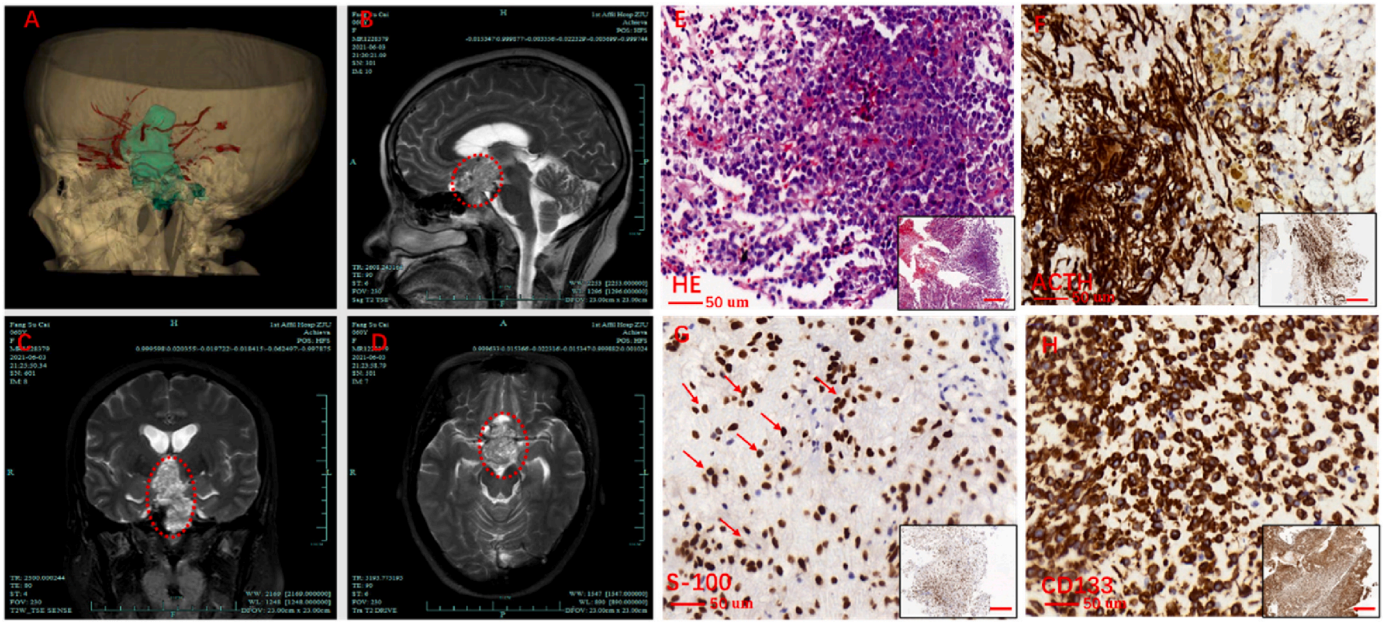

Fig. 2. Surgical removal of the tumour and Isolation of FS cells and tumour stem cells from a patient with invasive pituitary adenoma. A) Radiological 3D reconstruction of morphology from invasive pituitary adenoma Patients (tumour green); B-D) T2-weighted MRI scans of a giant pituitary adenoma(marked as red circle) (B: sagittal view; C: coronal view D: axial view); E) HE stanning of tumour section (scare bar 50um left, 200 μm right); F) The histopathological diagnosis indicated and ACTH-positive pituitary adenoma (scare bar 50um left, 200 μm right); G) S100-positive folliculostelate cells (scare bar 50um left, 200 μm right); H); Detection of CD133 expression in tumour tissue (scare bar 50um left, 200 μm right). (For interpretation of the references to color in this figure legend, the reader is referred to the Web version of this article.)

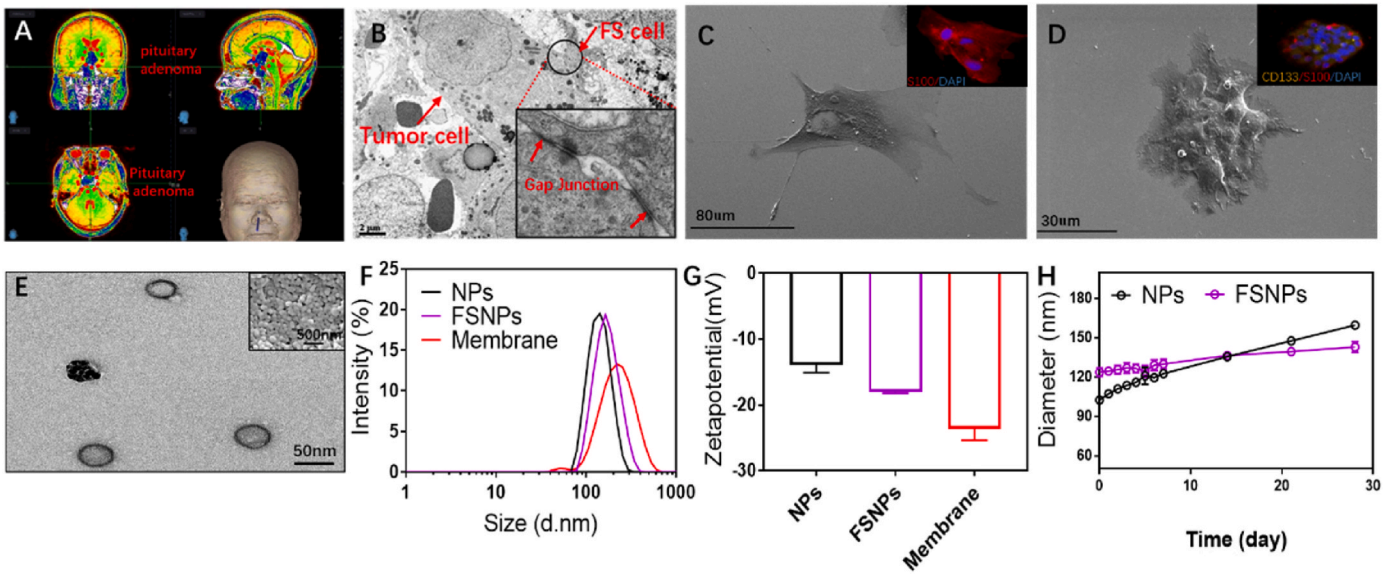

Fig. 3. Synthesis and characterization of FSNPs. A) patient underwent the transsphenoidal surgery by MR imaging neuronavigation; B) Gap junctions between tumour cells and FS cells; C) morphology of cultured FS cells after flow sorting; D) morphology of tumour stem cells. E) Representative image of FSNPs as captured by SEM (scare bar: 50 nm (insert 500 nm)) and TEM (insert, scare bar: 100 nm); F) DLS analysis of the hydrodynamic diameters of NPs, FSNPs and Membrane; G) Zeta potential of cell membrane and the indicated NPs (n = 3); H) Stability of NPs and FSNPs in serum-containing medium over 28 days (n = 3).

membranes of FS neurones [39]. To mimic the bidirectional interactions, we fabricated PLGA NPs with a surface coating on the FS cell membrane. PLGA NPs were synthesised using a standard emulsion, and FS cell membranes were prepared by gradient centrifugation after freeze-thaw and sonication processes. The resulting FS cell membrane-coated NPs or FSNPs were spherical in morphology and in size of 120 nm observed by scanning electron microscope (Fig. 3-E insert). Transmission electron microscopy (TEM) analysis showed that

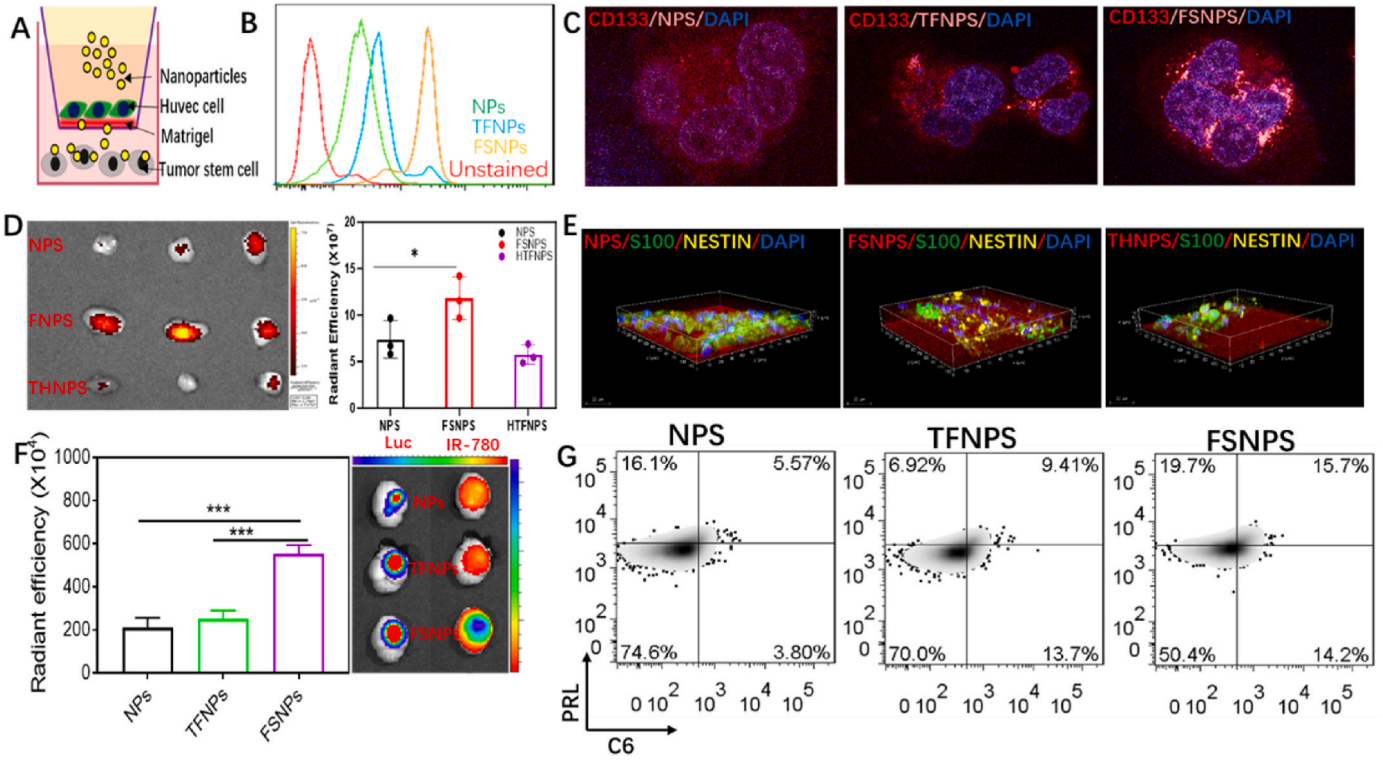

Fig. 4. FSNPs mediated enhanced permeability and retention (EPR) effects. A) Sketch map of tumour microenvironmental vasculature mimicking co-culture system; B) Flow analysis of uptake of indicated nanoparticles by tumour stem cells in the bottom chamber after 4 h; C) Intracellular distribution of Rhodamine loaded nanoformulations in the bottom chamber as captured by confocal (Red: CD133, Pink: NPs); D) Quantification and biodistribution of IR-780 loaded nanoparticles in the tumour from heterotopic pituitary adenoma model; E) Representative images of the distribution of NPS, FSNPs, THNPs in the tumour region (Red: nanoformulations, Green: S100, Yellow: Nestin, Blue: DAPI); F) Quantification and distribution of IR-780 encapsulated nanoformulations in orthotopic pituitary adenoma model; G) Flow analysis of the specificity of accumulation of nanoformulations in single tumour cells form tumour. (For interpretation of the references to color in this figure legend, the reader is referred to the Web version of this article.)

FMNPs had a visible core-shell structure compared to naked NPs (Fig. 3 E and Supplemental Figure 1 F). Furthermore, SDS-PAGE was performed to observe the transfer of FS cell membrane proteins to the FSNPs (Supplemental Figure 2). Quantification of the hydrodynamic diameter by dynamic light scattering (DLS) revealed that the FSNPs were slightly larger than the naked NPs (Fig. 3-F). Compared to the uncoated NPs, the FSNPs were more negatively charged, which could be attributed to the cell membrane (Fig. 3 G). Over time, the FSNPs were more stable than the naked NPs in a serum-containing medium (Fig. 3H).

3.3. Enhanced EPR effects by FS cell membrane coating

To mimic the tumour microenvironment, a Transwell co-culture of tumour stem cells in the bottom chamber and human umbilical vein endothelial (Huvec) cells with Matrigel in the upper chamber was performed to detect the vascular permeability of the nanoformulations *in vitro* (Fig. 4 A). 100ug of Rhodamine-loaded NPs, tumour-associated fibroblasts (another component from pituitary tumour stroma) membrane-coated NPs (or TFNPs), and FSNPs were added and incubated in up chamber for 4 h. The characterisation of tumour-associated fibroblasts and TFNPs is shown in Supplemental Fig. 2 A, B, and C. After incubation, the cells from the bottom chamber were collected to analyse the uptake of the indicated nanoparticles using flow cytometry. The internalisation of nanoparticles increased after coating with the cell membrane, indicating that the stromal cell membrane coating could improve the vasculature permeability of nanoparticles. Coating with the FS cell membrane was more significant for enhanced permeability than modification with tumour associated fibroblasts (Fig. 4 B). This was further confirmed by observing the intracellular distribution of nanoformulations with immunocytochemistry staining of CD133 by confocal microscopy at 496 nm excitation and 520 nm emission (Fig. 4C).

Next, we evaluated the tumour-targeting efficiency of our nanoformulations for heterotopic pituitary adenoma *in vivo*. The NPs, TFNPs, and FSNPs were synthesised by encapsulation IR-780. The resulting nanoformulations were administered to mice bearing front pituitary adenomas inoculated with patient-derived tumour stem cells. After 50 h, the mice were imaged using IVIS and euthanised (Supplemental Figure S4 A and B). The tumour tissues and main organs were harvested and subjected to imaging and quantification of IR-780 radiant efficiency. Consistent with the *in vitro* performance, coating with tumour stromal cell membranes improved the accumulation of nanoparticles in the tumour tissue (Fig. 4 D left). Quantification of IR780 fluorescence revealed that FSNPs accumulated in the tumour tissue in efficiency 1.6 and 2.05 times greater than naked NPs and TFNPs, respectively, indicating that an enhanced EPR effect could be achieved *in vivo* by presenting FS cell membranes on the surface of the nanoparticles (Fig. 4 D right). Furthermore, the tumours were frozen, sliced, and stained with NESTIN and S100 to detect the density of nanoparticles in the tumour tissues. We found that the FSNPs had a much higher density than the NPs and THNPs, illustrating the enhanced EPR effect of our strategy (Fig. 4 E and Supplemental Fig. 5 A and B).

Next, to verify whether the FSNP-mediated enhancement of the EPR effect could be duplicated in orthotopic pituitary adenoma, we first engineered cancer stem cells to express luciferase through lentiviral transduction (supplemental Figure S6 a and b) and implanted them intracranially in nude mice. IR-780 loaded NPS, TFNPs, and FSNPs were administered through tail vein injection after verification of the luciferase signal. 24 h after administration, the mice were euthanised, and their brains were harvested for imaging. As expected, the accumulation of FSNPs in the brain was mainly located in the tumour region with high efficiency (Fig. 4 F right). Quantification of the IR-780 radiant signal demonstrated that FSNPs accumulated in the tumour region with efficiency 7.8 and 6.5 times greater than that of the NPs and TFNPs (Fig. 4F left). To further analyse the specificity of tumour accumulation of nanoformulations at the single-cell level, tumours from the brain were surgically isolated, sectioned, and enzymatically digested into single cells by trypsin for *in vivo* uptake analysis by flow cytometry after the injection of coumarin-6 incapsulated nanoformulations for 24 h. The results reflected that the amounts of ACTH and coumarin-6 double-positive cells from mice that received FSNPs are about 2.8 and 1.6 times higher than naked NPs and TFNPs, demonstrating the superior tumour penetration capacity of FSNPs (Fig. 4 G, Supplemental Figure 7). These results suggest that coating with tumour stroma cell-derived membranes could help improve the EPR effects, thus enhancing the accumulation of nanoparticles in pituitary adenoma both heterotopically and orthotopically.

3.4. Therapeutic efficacy of mitotane-loaded FSNPs for heterotopic pituitary adenoma

Next, we assessed the FSNPs for the targeted delivery of therapeutics for heterotopic invasive pituitary adenomas. Mitotane, an anticortisolic drug proven safe and effective in patients with invasive pituitary adenomas [38,40,41], was encapsulated and evaluated in heterotopic pituitary adenomas. Mitotane-loaded FSNPs or M-FSNPs were synthesised at a loading of 10 % by weight. Mitotane encapsulation did not alter the morphology of FSNPs of similar size (Supplemental Fig. 8 A and B). M-FSNPs released over 33.6 % of the Mitotasne in PBS over 72 h in a controlled manner (Fig. 5 A). A heterotopic pituitary adenoma model was established and assigned to four groups that received treatment with M-FSNPs, free mitotane, empty FSNPs, or a PBS control. Treatments were performed 2 times a week at a dose of 10 mg/kg until the tumour volume reached 1500 mm^3. Free Mitotane was administrated at 100ug/kg. During treatment, mice were monitored for tumour growth and weight changes (Fig. 5 B–C, Supplemental Figure 9). We found that tumour growth in the free mitotane-treated group was slightly suppressed, whereas the M-FSNPs showed significant tumour inhibition. The remission rates in mice treated with free Mitotane and M-FSNPs were 30 % and 79 %, respectively, compared to 4 % in mice treated with empty FSNPs compared to mice treated with PBS. We also calculated the survival rate of each group as determined by death when the individual tumour volume reached 1500 mm^3. Consistently, the injection of mitotane showed modest control of tumour growth, extending the median survival from 28 months in the PBS group to 35. The M-FSNP group showed significant tumour suppression, with a median survival of 29 for the empty-FSNP group to 49 (Fig. 5 D). In line with the treatment scheme, serum corticosterone levels were monitored on days 7, 14, 21, and 29 to evaluate the control of Cushing syndrome. The results showed that the administration of M-FSNPs successfully balanced blood corticosterone levels in the invasive pituitary adenoma (Fig. 5E). Furthermore, massive apoptosis of tumour cells, induced by M-FNPs, was detected by pathological examination with HE and TUNEL staining (Fig. 5 F and G). With the enhanced EPR effects for tumour targeting, FSNPs can be designed as a drug delivery system for heterotopic pituitary adenomas with high therapeutic efficacy when loaded with mitotane.

4. Conclusion

In summary, we developed a new tumour stroma cell-mimicking system for invasive pituitary adenomas. Intrigued by the cellular ultrastructure evidence of gap junctions between folliculostellate cells and tumour cells from patient-derived tumour tissue, we isolated tumour stoma cells and FS cells specifically for the synthesis of FS cell membrane-coated NPs to mimic the bidirectional interactions between tumour stoma and tumour cells in the pathophysiological microenvironment of invasive pituitary adenoma. We discovered that the resulting FSNPs could enhance the EPR effects for tumour-targeted delivery both *in vitro* and *in vivo*. We further demonstrated that FSNPs significantly enhanced the efficacy of Mitotane for Invasive pituitary adenomas. In addition to heterotopic pituitary adenomas, M-FSNPs are also effective for treating orthotopic pituitary adenomas. Because of their excellent

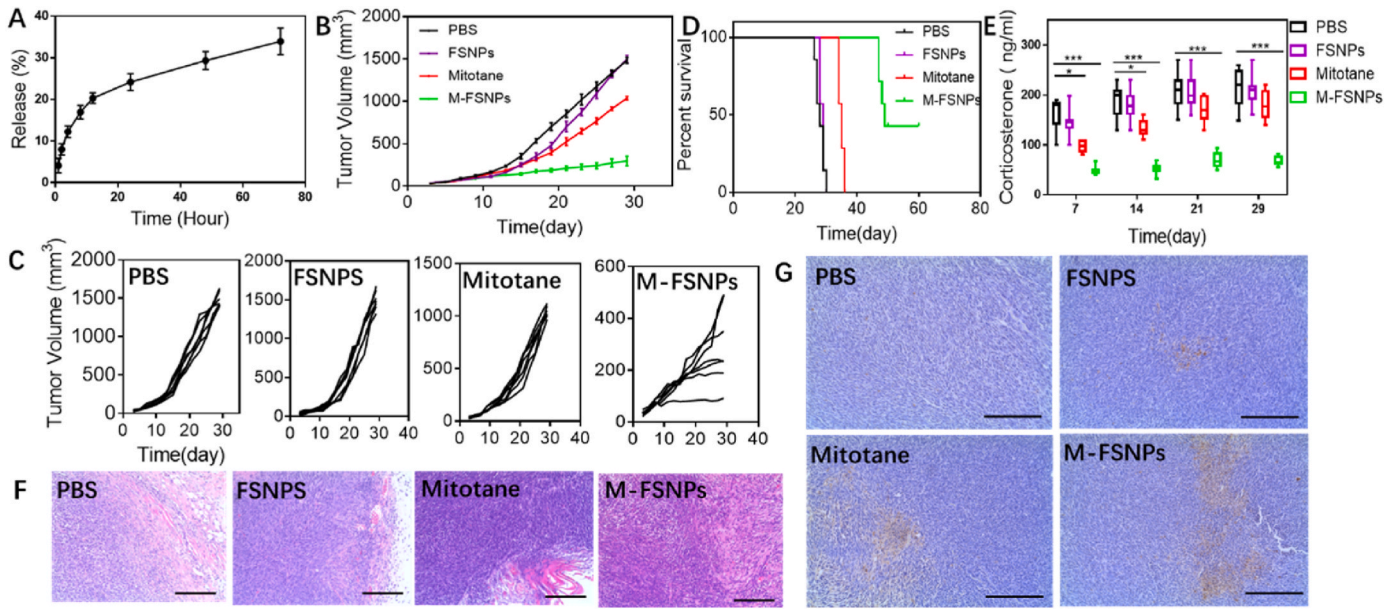

Fig. 5. Characterization of therapeutic efficacy of Mitotane-loaded FSNPs for heterotopic Invasive pituitary adenoma. A) Cumulated release of Mitotane from M-FSNPs with time n = 3; B) Change of tumour volumes on average in mice received the indicated treatment (n = 7; mean ± SD); C) Individual tumour growth kinetics for indicated group; D) Kaplan-Meier survival curves of mice received PBS, FSNPs, Mitotane, and M-FNPs (n = 7); E) Continuous monitoring of serum corticosterone paralleled with mice receive indicated treatment (n = 7); F) HE staining of tumour section after treatment; G) immunohistochemical staining of tunel from tumour tissue in each group.

therapeutic benefits, mitotane-encapsulated FSNPs have the potential to be translated into clinical applications for the management of patients with invasive pituitary adenoma.

Credit author statement

Junning Ma: Conceptualization, Data curation, Formal analysis, Funding acquisition, Methodology, Resources, Supervision, Validation, Visualization, Writing – original draft, Writing – review & editing. **Yin Wei:** Data curation, Resources, Validation. **Xiaojian Zhang:** Data curation, Funding acquisition, Resources. **Lu Lin:** Data curation, Formal analysis, Methodology, Resources, Lisi Dai, Methodology, Resources. **Youmei Bao:** Data curation, Investigation, Software. **Hui Cao:** Data curation, Methodology, Resources. **Honghwei Chen:** Data curation, Methodology. **Jianbo Yu:** Data curation, Formal analysis. **Jiqi Yang:** Data curation. **Yue Zhang:** Data curation. **Huimin Lan** helps to culture and take care of animal medel.**XueYang Li:** Data curation. **Huang Qiong:** Data curation. **Dan Yang:** Data curation. **Yajun Yu:** Data curation. **Jingyao Chen:** Data curation. **Chengchen Zhang:** Data curation. **Li liu** helps to take the confocal image.**Lei Chen:** Data curation. **Renya Zhan:** Visualization. **Fei Liu:** Visualization.

Declaration of competing interest

The authors declare that they have no known competing financial interests or personal relationships that could have appeared to influence the work reported in this paper.

Data availability

The data that has been used is confidential.

Acknowledgements

This study was supported by The National Natural Science Foundation of China (Grant No. 8210110115), and China Postdoctoral Science Foundation (Grant No.2021M692798).

We also give special appreciation to Xiaomin Zhang, Huanming Qian, and Jin Niu from the Center of Electron Microscopy, Zhejiang University, Life Science Division and Core Facilities, and Zhejiang University School of Medicine for their technical support. We appreciate YaJun Yu, Chengcheng Zhang, Dan Yang, Sanhua Fang, Jingyao Chen, Li Liu and Ming Xiao from the Core Facilities, Zhejiang University School of Medicine for their technical support.We also give appreciate to Wenkai Zhang, Yanzhe Wang, Huimin Lan, Xiaoyu Feng, Jie Dong, and Li Xiao from Guangdong Provincial Key Laboratory of Biomedical Imaging, Fifth Affiliated Hospital Sun Yat-sen University.

All animal procedures complied with the guidelines of the Institutional Animal Care and Use Committee of Zhejiang Province. We also thank Yue Chen and Jiangxun Heng from the College of Environmental and Resource Sciences, Zhejiang University. We also thank Prof. Peidong Han and his research team at the Zhejiang University School of Medicine. We also give special appriciate to Principal Song Gao from Sunyat-Sen University, Principal Jiangfeng Du from Zhejiang University, Secretary of the Party Committee Shaobo Ren from Zhejiang University, Secretary of the Party Committee Chunshen Chen from Sunyat-Sen University. Special appriciate is also given to Hong Shan dean of the Fifth affliated hosipital SunYat-Sen University. We also appriciate Professor Penghong Song, Professor Yangwen Jiao from the First affliated hospital of ZheJiang University. We also give appriciate to Professor Xin Pen from the Fifth Affiliated Hospital of Sun Yat-Sen University. All medical research uses or analyses of human subjects complied with the guidelines of the World Medical Association (WMA) Declaration of Helsinki.

We also thank Beining Sa, Bingbing Wang, Yang Long, Li Zhen, Xiaofeng Bao, Zimeng Li, Xinyu Yan, Hui Kang, Tao Pan, Qiang Gang, Maitige Ni, Yinqi Wang, and Shaozhuo Gao of China Media Group. Special appreciation is also given to Cunyin Hua, Binwen Wang and Ning Mao,Chunyin and from the Ministry of Foreign Affairs. Special appreciation is also given to Fenglian Zhu from the Taiwan Affairs Office of the State Council.Special appreciation is also given to President Jinping Xi, Premier of China's State Council Qiang Li, Secretary of the Central and State Organs Working Committee Qi Cai, and National Commission of Supervision of the People's Republic of China Xi Li.

Appendix A. Supplementary data

Supplementary data to this article can be found online at https://doi.org/10.1016/j.mtbio.2023.100895.

References

[1] D.W. McMillin, J.M. Negri, C.S. Mitsiades, The role of tumour-stromal interactions in modifying drug response: challenges and opportunities, Nat. Rev. Drug Discov. 12 (3) (2013) 217–228.
[2] M. Kawada, Small molecules modulating tumor-stromal cell interactions: new candidates for anti-tumor drugs, J. Antibiot. (Tokyo) 69 (6) (2016) 411–414.
[3] M.M. Mueller, N.E. Fusenig, Friends or foes - bipolar effects of the tumour stroma in cancer, Nat. Rev. Cancer 4 (11) (2004) 839–849.
[4] I. Kola, The state of innovation in drug development, Clin. Pharmacol. Therapeut. 83 (2) (2008) 227–230.
[5] D.W. McMillin, J.M. Negri, C.S. Mitsiades, The role of tumour-stromal interactions in modifying drug response: challenges and opportunities, Nat. Rev. Drug Discov. 12 (3) (2013) 217–228.
[6] I. Kola, The state of innovation in drug development, Clin. Pharmacol. Ther. 83 (2) (2008) 227–230.
[7] I. Kola, J. Landis, Can the pharmaceutical industry reduce attrition rates? Nat. Rev. Drug Discov. 3 (8) (2004) 711–715.
[8] J.A. DiMasi, H.G. Grabowski, Economics of new oncology drug development, J. Clin. Oncol. 25 (2) (2007) 209–216.
[9] C. Zhang, J. Ren, J. Hua, L. Xia, J. He, D. Huo, et al., Multifunctional Bi(2)WO(6) nanoparticles for CT-Guided photothermal and Oxygen-free photodynamic therapy, ACS Appl. Mater. Interfaces 10 (1) (2018) 1132–1146.
[10] R.X. Zhang, J. Li, T. Zhang, M.A. Amini, C.S. He, B. Lu, et al., Importance of integrating nanotechnology with pharmacology and physiology for innovative drug delivery and therapy - an illustration with firsthand examples, Acta Pharmacol. Sin. 39 (5) (2018) 825–844.
[11] R. van der Meel, E. Sulheim, Y. Shi, F. Kiessling, W.J.M. Mulder, T. Lammers, Smart cancer nanomedicine, Nat. Nanotechnol. 14 (11) (2019) 1007–1017.
[12] L. Hong, S. Jiang, S. Granick, Simple method to produce Janus colloidal particles in large quantity, Langmuir 22 (23) (2006) 9495–9499.
[13] Z.D. Lei, L. Ding, C.J. Yao, F.F. Mo, C.C. Li, Y.A. Huang, et al., A highly efficient tumor-targeting Nanoprobe with a novel cell membrane permeability mechanism, Adv. Mater. 31 (12) (2019).
[14] C. Zhang, J. Ren, J. He, Y. Ding, H. Da, Y. Hu, Long-term monitoring of tumor-related autophagy by FeO-NO• nanoparticles, Biomaterials 179 (2018) 186–198.
[15] S. Kunjachan, R. Pola, F. Gremse, B. Theek, J. Ehling, D. Moeckel, et al., Passive versus active tumor targeting using RGD- and NGR-Modified polymeric nanomedicines, Nano Lett. 14 (2) (2014) 972–981.
[16] M. Juweid, R. Neumann, C. Paik, M.J. Perez-Bacete, J. Sato, W. van Osdol, et al., Micropharmacology of monoclonal antibodies in solid tumors: direct experimental evidence for a binding site barrier, Cancer Res. 52 (19) (1992) 5144–5153.
[17] F. Danhier, To exploit the tumor microenvironment: since the EPR effect fails in the clinic, what is the future of nanomedicine? J. Contr. Release 244 (2016) 108–121.
[18] S. Taurin, H. Nehoff, K. Greish, Anticancer nanomedicine and tumor vascular permeability; where is the missing link? J. Contr. Release 164 (3) (2012) 265–275.
[19] R.H. Fang, A.V. Kroll, W. Gao, L. Zhang, Cell membrane coating nanotechnology, Adv. Mater. 30 (23) (2018), e1706759.
[20] J. Hu, X.W. Yuan, F. Wang, H.L. Gao, X.L. Liu, W. Zhang, The progress and perspective of strategies to improve tumor penetration of nanomedicines, Chin. Chem. Lett. 32 (4) (2021) 1341–1347.
[21] C.M. Hu, L. Zhang, S. Aryal, C. Cheung, R.H. Fang, L. Zhang, Erythrocyte membrane-camouflaged polymeric nanoparticles as a biomimetic delivery platform, Proc. Natl. Acad. Sci. U. S. A. 108 (27) (2011) 10980–10985.
[22] C. Hu, T. Lei, Y.Z. Wang, J. Cao, X.T. Yang, L. Qin, et al., Phagocyte-membrane-coated and laser-responsive nanoparticles control primary and metastatic cancer by inducing anti-tumor immunity, Biomaterials 255 (2020).
[23] R. Liu, Y. An, W.F. Jia, Y.S. Wang, Y. Wu, Y.H. Zhen, et al., Macrophage-mimic shape changeable nanomedicine retained in tumor for multimodal therapy of breast cancer, J. Contr. Release 321 (2020) 589–601.
[24] H. Zuo, J. Tao, H. Shi, J. He, Z. Zhou, C. Zhang, Platelet-mimicking nanoparticles co-loaded with W(18)O(49) and metformin alleviate tumor hypoxia for enhanced photodynamic therapy and photothermal therapy, Acta Biomater. 80 (2018) 296–307.
[25] M.D. Ilie, A. Vasiljevic, G. Raverot, P. Bertolino, The microenvironment of pituitary tumors-Biological and therapeutic implications, Cancers 11 (10) (2019).
[26] W. Allaerts, H. Vankelecom, History and perspectives of pituitary folliculo-stellate cell research, Eur. J. Endocrinol. 153 (1) (2005) 1–12.
[27] S. Hori, N. Hayashi, J. Fukuoka, M. Kurimoto, H. Hamada, K. Miyajima, et al., Folliculostellate cell tumor in pituitary gland, Neuropathology 29 (1) (2009) 78–80.
[28] D. Voit, W. Saeger, D.K. Ludecke, Folliculo-stellate cells in pituitary adenomas of patients with acromegaly, Pathol. Res. Pract. 195 (3) (1999) 143–147.
[29] I. Vajtai, A. Kappeler, R. Sahli, Folliculo-stellate cells of "true dendritic" type are involved in the inflammatory microenvironment of tumor immunosurveillance of pituitary adenomas, Diagn. Pathol. 2 (2007).
[30] T. Aasen, E. Leithe, S.V. Graham, P. Kameritsch, M.D. Mayan, M. Mesnil, et al., Connexins in cancer: bridging the gap to the clinic, Oncogene 38 (23) (2019) 4429–4451.
[31] Q. Xu, X. Yuan, P. Tunici, G. Liu, X. Fan, M. Xu, et al., Isolation of tumour stem-like cells from benign tumours, Br. J. Cancer 101 (2) (2009) 303–311.
[32] M. Orciani, S. Davis, G. Appolloni, R. Lazzarini, M. Mattioli-Belmonte, R. A. Ricciuti, et al., Isolation and characterization of progenitor mesenchymal cells in human pituitary tumors, Cancer Gene Ther. 22 (1) (2015) 9–16.
[33] J. Ma, S. Zhang, J. Liu, F. Liu, F. Du, M. Li, et al., Targeted drug delivery to Stroke via Chemotactic Recruitment of nanoparticles coated with membrane of engineered neural stem cells, Small (2019), e1902011.
[34] G. Strohbehn, D. Coman, L. Han, R.R.T. Ragheb, T.M. Fahmy, A.J. Huttner, et al., Imaging the delivery of brain-penetrating PLGA nanoparticles in the brain using magnetic resonance, Journal of neuro-oncology 121 (3) (2015) 441–449.
[35] J. Zhou, T.R. Patel, R.W. Sirianni, G. Strohbehn, M.-Q. Zheng, N. Duong, et al., Highly penetrative, drug-loaded nanocarriers improve treatment of glioblastoma, Proc. Natl. Acad. Sci. U. S. A. 110 (29) (2013) 11751–11756.
[36] Y. Chen, X. Gou, D.K. Kong, X. Wang, J. Wang, Z. Chen, et al., EMMPRIN regulates tumor growth and metastasis by recruiting bone marrow-derived cells through paracrine signaling of SDF-1 and VEGF, Oncotarget 6 (32) (2015) 32575–32585.
[37] H. Raff, J.W. Findling, A physiologic approach to diagnosis of the Cushing syndrome, Ann. Intern. Med. 138 (12) (2003) 980–991.
[38] N.A. Tritos, B.M. Biller, B. Swearingen, Management of Cushing disease, Nat. Rev. Endocrinol. 7 (5) (2011) 279–289.
[39] M.L. Vitale, A. Barry, Biphasic effect of basic fibroblast growth factor on anterior pituitary folliculostellate TtT/GF cell Coupling, and connexin 43 expression and Phosphorylation, J. Neuroendocrinol. 27 (10) (2015) 787–801.
[40] G.D. Satyarthee, D.R. Sawarkar, Management of Cerebral Venous and Sinus Thrombosis following transsphenoidal surgery for Cushing disease during Early Postoperative Period: Uncommon Neurosurgical Complication, World Neurosurg 111 (2018) 422.
[41] M.K. Aghi, Management of recurrent and refractory Cushing disease, Nat. Clin. Pract. Endocrinol. Metabol. 4 (10) (2008) 560–568.